

Full Length Article

Aging of 2D MXene nanoparticles in air: An XPS and TEM study



Matej Mičušík ^{a,*}, Miroslav Šlouf ^b, Anastasiia Stepura ^a, Yaryna Soyka ^a, Evgeni Ovodok ^c, Michal Procházka ^a, Mária Omastová ^a

^a Polymer Institute SAS, Dúbravská cesta 9, 84541 Bratislava, Slovakia

^b Institute of Macromolecular Chemistry, Czech Academy of Sciences, Heyrovského nám. 2, 162 06 Prague 6, Czech Republic

^c Research Institute for Physical and Chemical Problems of the Belarusian State University, Minsk, Belarus

ARTICLE INFO

Keywords:
MXene
Surface chemistry
Stability in air
2D nanomaterials
XPS
TEM-EDX-SAED

ABSTRACT

Different batches of $Ti_3C_2O_x$ MXene were prepared, and their stability in air and argon was studied. X-ray photoelectron spectroscopy (XPS) and transmission electron microscopy (TEM) in multiple modes (bright field imaging, energy-dispersive X-ray analysis, and selected-area electron diffraction) was employed to study the chemical and morphological changes in two-dimensional (2D) MXene exposed to air for several days and months. We observed the progressive development of the Ti^{4+} state accompanied by the development of TiO_2 formation, which lead to a slow disintegration of the 2D MXene nanosheets, although their overall morphology and crystalline structure can persist for several months. The presence of water is found to play an important role in the hydrolysis and degradation reactions during MXene aging. Our XPS and TEM studies show how the surface chemistry changes during aging in air and which surface termination groups are indicative of stable $Ti_3C_2O_x$ MXene and which storage conditions can stabilize MXene for more than 337 days.

1. Introduction

Two-dimensional (2D) materials have drawn attention in many scientific areas due to their extraordinary electronic, mechanical and optical properties, which originate from their 2D morphology connected with the very low thickness. The best-known 2D material is graphene. MXene is one of many forms of 2D structure. The general formula for MXenes is $M_{n+1}X_nT_x$ ($n = 1-3$), where M represents a transition metal (Sc, Ti, Zr, Hf, V, Nb, Ta, Cr, Mo, and others), X is carbon and/or nitrogen and T_x refers to various functional groups on the surface (e.g., OH, O, F, etc.).

MXene shows interesting properties, and various possible applications of these 2D materials in supercapacitors [1,2], Li batteries [3,4], sensors [5], optoelectronics [6], solar cell devices [7] and many others have been reported in the literature.

MXene sheets are terminated with various functional groups, such as $-OH$, $=O$ and $-F$. This makes these 2D materials hydrophilic and stable in aqueous dispersions. Unlike other 2D materials, such as graphene, MXenes have hydrophilic surfaces and high metallic conductivities ($\sim 6000-8000$ S/cm) [8–10]. On the other hand, one of the main drawbacks of MXene in applications is its relatively low stability after reactions with water and oxygen, leading to decreased stability in air

[11]. MXene preparation includes severe chemical etching, which can generate defects on the surface of the MXene sheet. Defects and vacancies on the surface are then vulnerable to oxidation. MXene ($Ti_3C_2T_x$) was first reported in 2011 by Naquib et al. by etching the MAX phase (Ti_3AlC_2) with a strong HF acid [12]. Various methods involving HF etching have been reported for different types of MXenes [13,14]. Substantial improvement has been achieved with less severe etching conditions, where for etching of Al from the MAX phase of Ti_3AlC_2 , a mixture of LiF and HCl has been used [14]. This method is usually described as minimal intensive layer delamination (MILD) because the in situ formed HF is not that destructive to the MXene structure and Li^+ ions facilitate better intercalation, resulting in a clay-like structure composed of a few MXene layers with higher yields with no need for additional sonication [15]. This MILD method is now widely used, and the intercalation effectiveness can be improved by adding polar organic agents, such as hydrazine, urea, isopropylamine [16,17], or larger organic bases, such as tetrabutylammonium hydroxide (TBAOH), *n*-butylamine, choline hydroxide, etc. [18]. The MILD method with a tuned molar ratio of LiF and HCl leads to high-quality intercalated few-layer MXenes [8].

Iqbal et al. [19] reviewed the nature of the oxidation and degradation of MXenes and recent progress for controlling the oxidation

* Corresponding author.

E-mail address: matej.micusik@savba.sk (M. Mičušík).

kinetics. It is clear that HF acid can etch some exposed Ti atoms and create Ti vacancies, which are mostly present on the surface, and the inner Ti layer close to the carbon layer is less affected [20]. This is why a weaker acidic concentration during the MILD method leads to a less defective structure than for the case of strong acidic concentrations.

Our study aims to widen the knowledge for the surface chemistry of the most common $Ti_3C_2O_xF_x$ MXene and the change in chemical structure during aging in air. Surface chemistry is very important owing to the stability of the MXene structure over time. Atomic defects created during the chemical synthesis of MXenes clearly serve as a nucleation site for MXene oxidation [21]. Our XPS and TEM studies show how the surface chemistry changes during aging in air and which surface termination groups are indicative of stable $Ti_3C_2O_xF_x$ MXene and which storage conditions can lead to stable MXene. We also compare MXenes prepared by the MILD method with or without the presence of Li^+ left behind from the etching process and discuss the effect of impurities on the overall stability of the prepared MXene paste as well as delaminated 2D MXenes. To our best knowledge this is the first study comparing different batches of $Ti_3C_2O_xF_x$ MXenes containing various amounts of impurities.

2. Experimental

2.1. MXene preparation

$Ti_3C_2T_x$ MXene paste (ML (multilayered) MXenes) was prepared using the MILD (minimally intensive layer delamination) method, where HF was created in situ. First, 9 M HCl was poured into a plastic bottle made of Teflon, which was then placed into a water bath with cold water and ice. Next, 5 g of LiF was slowly added. The blend was mixed at 400 rpm for ~3–5 min. After that, approx. 5 g of MAX phase (40 μm Ti_3AlC_2 – provided by Materials Research Center (MRC), Kyiv, Ukraine) was also slowly added, and this mixture was stirred at 35 °C for 24 h. On the next day, this solution was split into 4 plastic centrifugation tubes so that the same amount of solution was present in each tube, and a centrifugation cycle for 10 min at 5000 rpm was started. After the first centrifugation, the supernatant from all tubes was collected into a measuring cylinder and the volume recorded, and then after each third centrifugation, a small amount of the supernatant was taken for pH measurements. Then, the new portions of distilled water were poured into tubes, and the next cycle was started. In total, 30 centrifugation cycles were performed, e.g., 5 pH measurements, and the final pH value was approximately 5.1. We obtained MXene paste with a concentration of 54 wt% (MX3) and 8 wt% (MX4) $Ti_3C_2T_x$. Another MXene paste with concentrations of 52 wt% (MX1) and 77 wt% (MX2) was received from Drexel University, USA.

The $Ti_3C_2T_x$ dispersion (2DMX1) was prepared using multilayered $Ti_3C_2T_x$ MXene paste obtained from Drexel University, USA. Delamination of 1 g of $Ti_3C_2T_x$ was performed using 1 g of LiCl (purity ≥ 99 %, Sigma-Aldrich), and the mixture was diluted with 25 mL of deionized water and stirred overnight using a magnetic stirrer at 35 °C. After stirring, the mixture was transferred to a centrifugation tube and centrifuged at 3500 rpm for 10 min. After centrifugation, the supernatant was removed, and deionized water was added. This step was repeated several times until the supernatant shows a black color. In the next step, the centrifugation time was extended to 1 h and repeated several times until the supernatant showed a green color corresponding to a single-layered $Ti_3C_2T_x$ MXene dispersion, which was collected into a glass bottle. The centrifugation was repeated several times until the supernatant was no longer black in color. The final solution of single-layered $Ti_3C_2T_x$ dispersion was adjusted to the concentration of the final solution of $c = 7.5 \text{ mg/mL}$.

2.2. Characterization techniques

2.2.1. XPS analysis

XPS was performed using a Thermo Scientific K-Alpha compact XPS

system (Thermo Fisher Scientific, UK) equipped with a microfocused, monochromatic Al K α X-ray source (1486.68 eV). The spectra for the survey were acquired in constant analyzer energy mode with a pass energy of 200 eV. Narrow spectral regions were collected using a pass energy of 50 eV. Charge compensation was achieved with an Ar flood gun system. Thermo Scientific Avantage software, version 5.9929 (Thermo Fisher Scientific), was used for digital acquisition and data processing. The surface compositions (in atomic %) were determined by considering the integrated peak areas of the detected atoms and the respective sensitivity factor.

2.2.2. TEM analysis

TEM analysis was performed with a transmission electron microscope Tecnai G2 Spirit Twin 12 (FEI; Czech Republic), which was equipped with a detector for energy dispersive X-ray analysis (EDX; detector EDAX; Mahwah, NJ, USA). The samples for TEM microscopy were prepared by drop casting 2 μL of the MXene dispersion onto a standard TEM supporting copper grid covered with an electron transparent carbon film. After 10 min of solvent evaporation at ambient temperature, the excess solution was removed by contacting the bottom of the grid with a thin strip of filtration paper to avoid oversaturation and nanoprecipitation during the drying process. Then, the specimens were left to dry completely. After drying, the samples were transferred to a TEM microscope. All samples were observed at an accelerating voltage of 120 kV. Standard bright field imaging (TEM/BF) was used to characterize the morphology of the particles, energy-dispersive analysis of X-rays (TEM/EDX) was used to determine the elemental composition, and selected area electron diffraction (TEM/SAED) was used to verify the crystalline structure. The experimental electron diffraction patterns were transformed to 1D diffractograms (by means of ProcessDiffraction [22]) and compared with theoretical X-ray diffraction patterns (calculated with PowderCell [23]) for the expected crystal structures of MXene (the crystal structure was obtained from the study of Shi et al. [24], and the theoretically calculated powder diffractogram was found to be very similar to the experimental powder X-ray diffraction pattern obtained by an independent group of authors [17]).

3. Results and discussion

3.1. XPS analysis

Table 1 summarizes the different MXene dispersions, types of aging in air (or argon in one case) and characterization performed. MX1, MX2 and MX3 were left as a paste at approximately 22 °C and humidity of approximately 30–40 % in the dark. MXene paste means that after etching of the Al and cleaning, we obtained a viscous MXene dispersion with a varying MXene concentration (**Table 1**). For the case of MX1 paste, an additional cleaning step was performed, and no Al was detected by XPS (**Table 2**). Sample MX4 was drop cast onto a Si wafer

Table 1
Description of MXene samples.

Sample	Description (MXene concentration, wt.%)	Type of aging (in air, 22 °C)	Characterization
MX1	MXene paste (52)	as a paste	XPS,
MX1- TEM	MXene paste (52)	dried on a carbon grid	TEM, SAED, EDX
MX2	MXene paste (77)	as a paste	XPS
MX2*- TEM	MXene paste (77)	as a paste in fridge (−20 °C)	XPS
MX3	MXene paste (54)	as a paste	XPS,
MX3- TEM	MXene paste (54)	dried on a carbon grid	TEM, SAED, EDX
MX4	MXene paste (8)	dried drop casted film	XPS
2DMX1	delaminated MXene (0.75)	dried drop casted film	XPS

Table 2

Surface chemical composition of the MAX phase and MXene samples as determined by XPS.

Sample	Surface chemical composition [at.%]					
	C 1s	O 1s	Ti 2p	F 1s	Li 1s/Cl 2p/N 1s/Al 2p	
MAX phase	34.1	37.4	16.5	—	—/0.6/—/11.5	
MX1	33.5	19.8	29.8	13.1	—/1.9/2.0/—	
MX2	32.2	13.1	32.1	15.2	—/1.7/1.3/2.3	
MX3	31.1	19.6	30.8	11.5	2.4/3.4/1.2/—	
MX4	16.2	6.6	9.3	28.1	37.6/1.1/0.8/0.3	
2DMX1	32.4	20.2	31.0	12.9	—/2.3/1.3/—	

and dried, and this MXene film was left in the dark at a temperature of approximately 22 °C and humidity of approximately 30–40 %. 2DMX1 is a delaminated MX1 dispersion prepared by the additional delamination step described in the experimental section. This 2DMX1 dispersion was drop cast onto a Si wafer and left in the dark at a temperature of approximately 22 °C and a humidity of approximately 30–40 %. MX2* is an MXene paste that is the same as MX2 but stored in a refrigerator at −20 °C. All MXenes were prepared by the MILD method under the same experimental conditions. The difference was in the method of purification, where for the case of samples MX3 and MX4, we detected a certain amount of Li⁺ and LiF arising from the MILD etching reactions (Table 2). The idea was also to evaluate the stability behavior for MXenes containing Li⁺ or excess LiF, which can be interesting for certain applications [25]. As is obvious from Table 2 and Fig. 1, after etching of the MAX phase, the Al2p signal at approximately 72–74 eV showed a substantial decrease or completely disappeared.

First, we compared the stability of MX3 (4) paste in air and in an Ar atmosphere. From the XPS high-resolution spectra, we could follow the changes in the chemistry of titanium (Ti 2p region) and carbon (C 1s region) and termination groups (F 1s and O 1s regions). As shown in Fig. 2a for the C 1s region, some adventitious carbon is visible as a result of some surface contamination as the sp³ carbon is centered at ~285.0 eV, C—O groups at ~286.2 eV and OC=O groups at ~288.9 eV [26]. The signal at ~284 eV (as shown in Fig. 2a as sp²) can originate from Ti-oxycarbides (Ti-OC) or graphitic carbon [27]. In MXenes, the presence of graphitic carbon can be attributed to the possible dissolution of Ti during etching, which can generate graphitic C—C formation [28]. C 1s at ~281.6 eV (see Fig. 2a) and at ~283 eV (in Table 3 as “C 1s II”) represents Ti₃C₂ signals [29].

Scheme 1 shows the possible termination groups of Ti₃C₂T_x, which can also be identified by XPS in Fig. 2 as C—Ti=O (O 1s at ~531.5 eV, in Table 3 as “O 1s I”), =Ti=O (O 1s at ~529.5 eV, in Table 3 as “O 1s ox”), Ti=F (F 1s at ~685.4 eV) and O=Ti=F/TiF₂ (F 1s at ~685.4 eV).

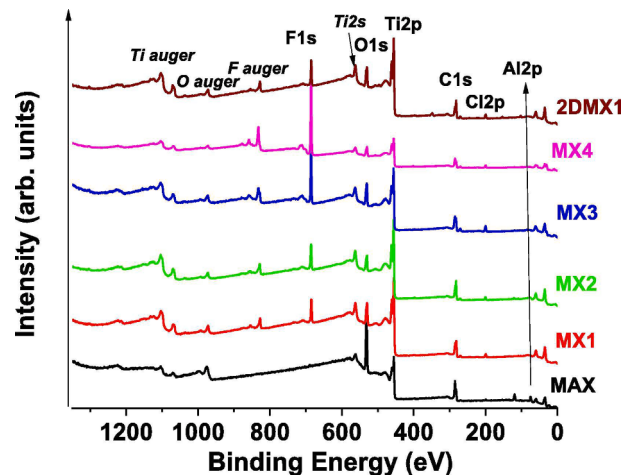


Fig. 1. XPS survey of the MAX phase and MXene samples.

The change in surface chemistry can also be followed in the Ti 2p region (Fig. 2c), where Ti 2p centered at ~458.5 eV can indicate the degradation of the Ti₃C₂ structure and the generation of TiO₂.

Table 3 shows that after 7 days in air, there is an increase in the amount of Li on the surface, which means that Li is not bonded and homogeneously distributed over the MXene structure but most likely migrates onto the surface, and, as a result, there is an increase in the initial Li content from 2.4 at.% to 10 at.%. After 7 days in air, an increase in the F 1s signal for O-Ti-F/TiF₂ is observed (Fig. 3a), and this type of signal dominates in the fluorine termination group and is accompanied by the oxidation of Ti (Fig. 3c). When compared to the aging in Ar, reduced contact with oxygen in the air shows no effect on suppressing the oxidation behavior (Fig. 3b,d). The sample is observed to be even more oxidized in Ar, but this difference can also be attributed to sample manipulation and sampling before the contents of the vial are exposed to the Ar atmosphere. This confirms the conclusions of Huang et al. [11] that the oxidation of Ti_x MXenes is mostly driven through hydrolysis, while direct oxidation by oxygen is less probable. Later, we will study only aging in air. To show the effect of Li ions, which can, for example, intercalate MXene layers and facilitate more intense hydrolysis, no Li is detected in MX2, as shown in Fig. 3e. After 14 days, we can see that without Li, intensive oxidation and generation of Ti⁴⁺ occurs, and, thus, formation of TiO₂ (as also confirmed by SAED, see Fig. 8).

A more stable dried film of the MX4 sample shows almost no change in the surface chemistry of oxygen (O 1s in Fig. 4a) after 57 days of aging in air, and a relatively narrow signal at ~529.5 eV corresponding to =O termination groups is still observed. These =O terminations possess higher energy formation in order to create Ti vacancies than for the case of -OH terminations of Ti₃C₂T_x MXene [20]. These -OH terminations are substantially hydrolyzed in the case of MX2 paste (Fig. 4b) because of the presence of water leading to much stronger oxidation and TiO₂ generation (Fig. 3e, Ti 2p at ~458.5 eV). Here, it is worth noting that for the case of MX4, the initial MXene concentration is lower. This implies that the MXene concentration in the MXene paste does not show a large effect, and the most important factor is the access to water during the aging time.

EDX for the MX1-TEM and MX3-TEM samples shows no reasonable difference after 4 months of aging in air, confirming the conclusion that impurities such as Li/LiF reactants and Al from the precursor do not influence the stability in air (see section 3.2.2 and discussion of TEM/EDX results therein).

The Ti 2p peak shape for the Ti carbides is asymmetric because of their electrical conductivity. Signals at ~455.6 eV (labeled as “Ti I” or Ti²⁺) and at ~456.7 eV (labeled as “Ti II” or Ti³⁺) can, therefore, be related to the asymmetry of Ti carbide or termination groups (Fig. 2c, Table 3). Then, the stoichiometry of MXene can be calculated from XPS measurements after subtracting the signals related to carbon contamination (C 1s signals above 284 eV) and TiO₂ signals (Ti 2p at ~458.5 eV). Fluorine termination groups can be calculated considering the F 1s signals related to Ti-F and O-Ti-F/TiF₂. For MX3 and MX4, we have not calculated the F-termination groups because they overlap with signals arising from LiF present in the MXene paste. This XPS stoichiometry has limited accuracy but can be indicative of the degradation of the Ti₃C₂T_x structure.

For the case of the MX2 and MX3 pastes, we can clearly observe an increase in the Ti/C ratio (Table 4) and an increase in the O/Ti ratio, as confirmed by EDX (see section 3.2.2 and TEM/EDX discussion therein). This confirms the disintegration of the MXene structure and the hydrolysis reactions leading to the production of gaseous CO₂, CH₄ and CO, as reported in [11].

We can also observe a decrease in the F/Ti ratio, indicating the oxidation of Ti-F termination groups through O-Ti-F, as shown in Fig. 3a.

On the other hand, samples aged as a dried film show no increase in the Ti/C ratio. When we drop cast and dry the delaminated 2DMX1 film, it is found to be very stable in air even after 83 days with no change observed in the Ti/C, O/Ti or F/Ti ratios. No change is observed in the

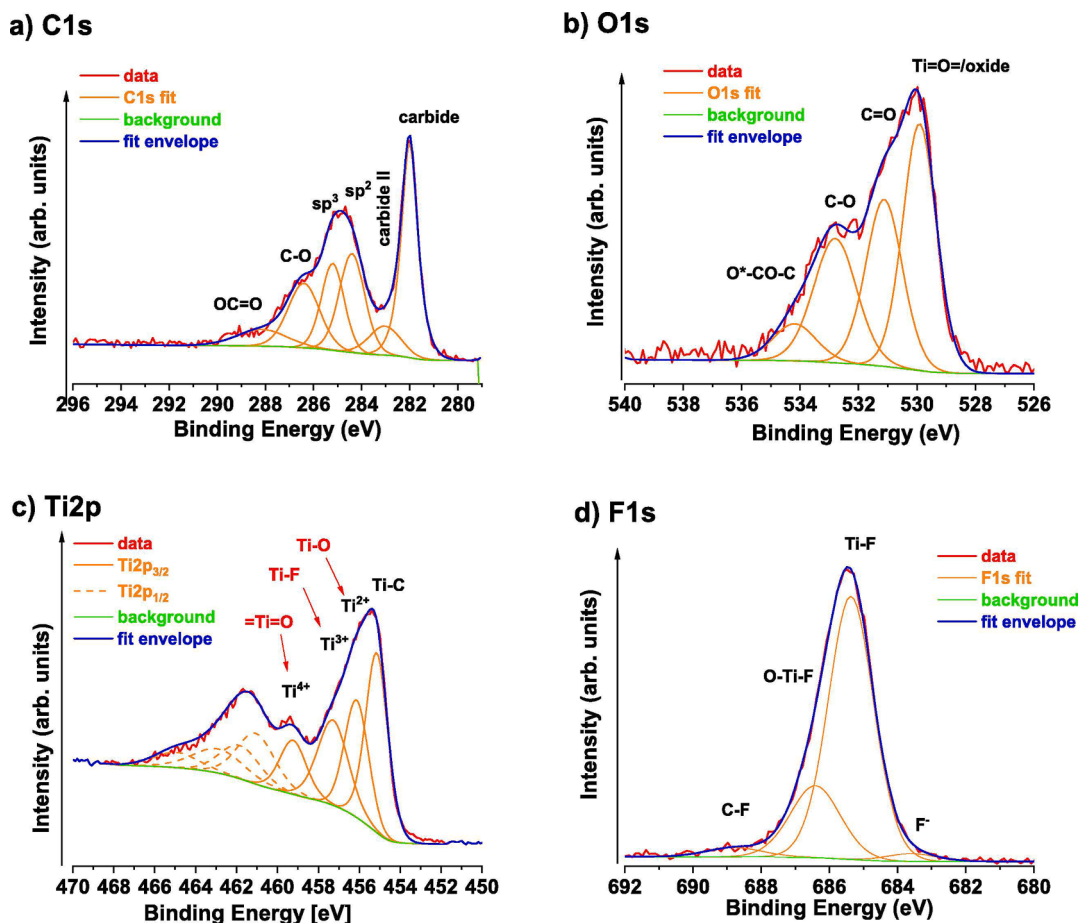


Fig. 2. XPS for MX3 in the a) C 1s region, b) O 1s region, c) Ti 2p region, and d) F 1s region.

Table 3
Surface chemical composition of aged MX3 samples in air.

MX3	Surface chemical composition (at.%)				
	C 1s	O 1s	Ti 2p	F 1s	Li 1s/Cl
Ti ₂ C ₂ /I/II/ sp ³ /CO/ OCO		ox/I/II/III	Ti ₃ C ₂ /I/II/ TiO ₂	F/TiF/ OTiF/ CF	2p/ N 1s/Al 2p
Day 0	31.1 14.8/3.2/4.2/ 5.3/2.5/1.1	19.6 9.7/5.5/ 3.7/0.7	30.8 11.6/7.3/ 7.9/4.0	11.5 1.0/8.1/ 1.8/0.6	2.4/3.4/ 1.2/—
Day 7	24.9 10.9/1.8/4.9/ 3.9/2.1/1.3	18.2 6.3/7.9/ 3.3/0.7	24.9 9.1/4.5/ 7.0/4.3	16.8 0.6/9.4/ 6.2/0.6	10.1/2.7/ 1.2/1.3
Day 27	21.4 6.1/1.1/4.5/ 6.1/2.1/1.5	24.7 14.8/5.3/ 3.9/0.7	20.9 5.2/3.3/ 3.7/8.7	17.9 0.4/4.9/ 12.2/0.4	9.5/2.2/ 0.8/2.7

surface chemistry, as shown in Fig. 5, where only a small increase in the Ti⁴⁺ signal at ~458.5 eV is visible.

To prevent hydrolysis in the MX2 paste, it is possible to decrease the storage temperature to -20 °C (sample MX2* in Table 4) by placing the MX2 paste into a refrigerator. In this way, the MX2 sample was observed to remain stable even after 337 days.

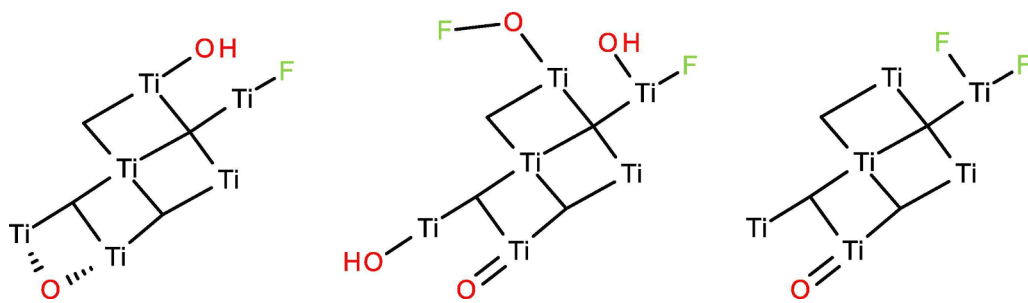
3.2. TEM analysis

Samples for TEM analysis were supplied in the form of MXene water suspensions in sealed flasks. After opening the flasks, the MXene sheets were deposited onto electron-transparent carbon films, as described

above in the Experimental section. The prepared samples were observed by TEM immediately after preparation and then after one month and four months. In the meantime, the MXene sheets were stored in a dry dark place in air at room temperature (~22 °C, 30–40 % humidity). Each TEM analysis comprised standard bright-field imaging (TEM/BF) to visualize the morphology of the MXene platelets, energy-dispersive X-ray spectroscopy (TEM/EDX) to quantify the elemental composition, and selected-area electron diffraction (TEM/SAED) to monitor the crystal structure. All experiments were repeated twice, with two MXene suspensions, which were obtained from two independent MXene syntheses (MX1-TEM and MX3-TEM in Table 1). The results of both experimental series are almost identical, and the results shown below are representative selections. The objective of all experiments was to supplement the XPS data shown in the previous section and to reveal how the aging of the MXene platelets in air impacts their morphology, elemental composition and crystalline structure.

3.2.1. TEM/BF: Impact of aging on MXene morphology

Fig. 6 shows representative TEM/BF micrographs of MX3-TEM as a function of time from sample preparation. The samples were prepared for TEM analysis from water suspensions (as described in the Experimental section) and contained both individual MXene platelets (Fig. 6a–c) and thicker MXene layers formed by overlapping platelets (Fig. 6d–f). The morphology of the individual MXene platelets (the upper row of Fig. 6) does not change with time; they remain compact, and their average size is maintained. The thicker MXene layers (the lower row in Fig. 6) yield quite intensive powder-like electron diffraction patterns with two strong diffraction peaks (the insets in the lower row of Fig. 6), whose overall appearance does not change either, although the intensity of the two main diffraction rings gradually fade



Scheme 1. Different chemical termination groups on the MXene structure.

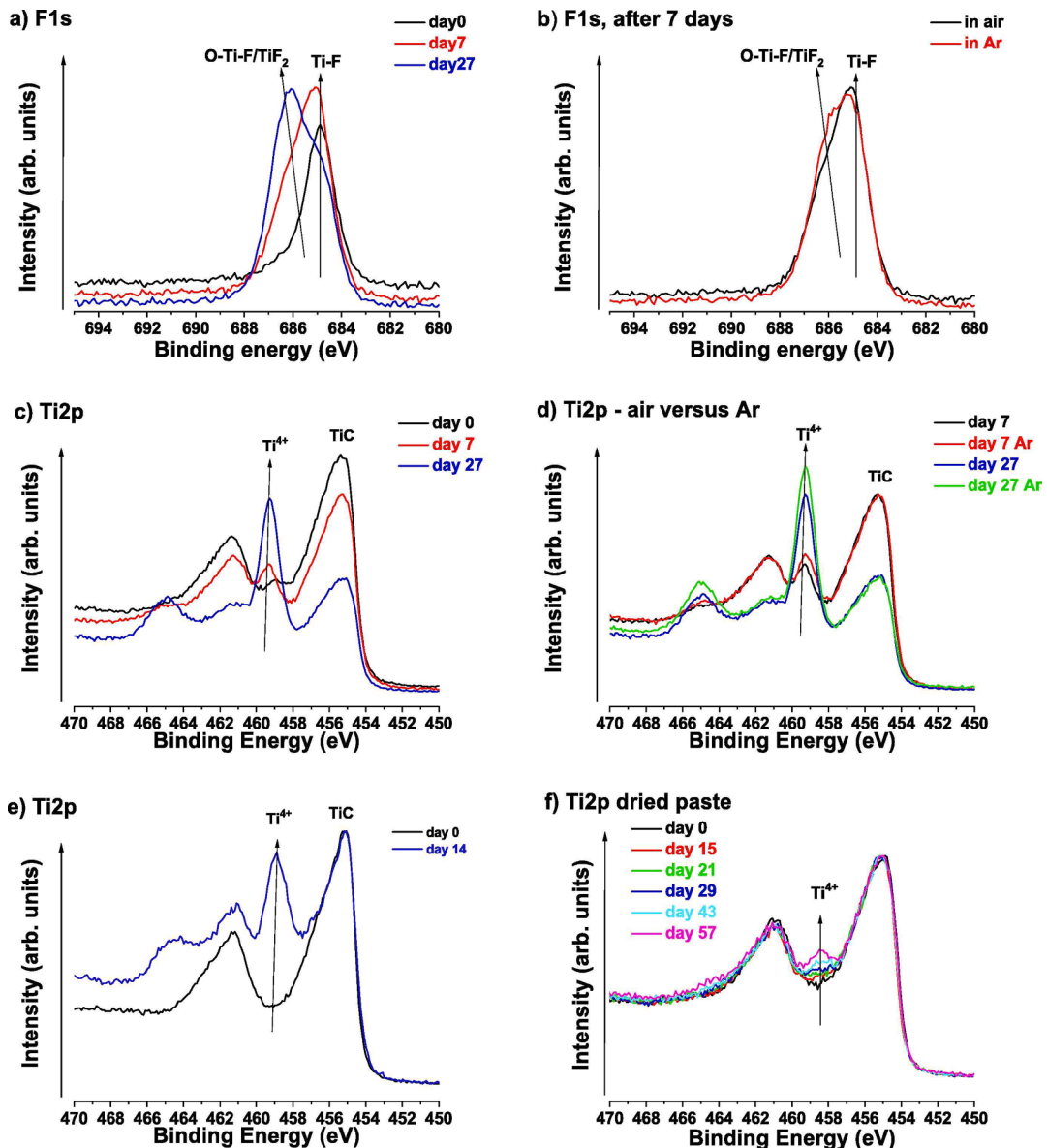


Fig. 3. XPS for several days of aging of the a) F 1s region of MX3 paste in air, b) F 1s region of MX3 paste in air and an Ar atmosphere, c) Ti 2p region of MX3 paste in air, d) Ti 2p region of MX3 paste in air and an Ar atmosphere, e) Ti 2p region of MX2 paste in air and f) Ti 2p region of MX4 (dried film) in air.

with time (we note that the contrast for the TEM/SAED patterns is normalized to the intensity of the primary beam, as documented by the roughly the same-sized central spot). This suggests that the crystalline structure of MXene is maintained, although it is somewhat deteriorated with time. The electron diffraction patterns are discussed below in the subsection dealing with the TEM/SAED results.

3.2.2. TEM/EDX: Impact of aging on MXene elemental composition

Fig. 7 summarizes the key results of the TEM/EDX analysis. A representative spectrum of MXene platelets (Fig. 7a) shows all expected elements: the components of the MXene platelets (Ti, C, O and F), the peaks arising from the supporting carbon-coated copper grid (C and Cu), a lower concentration of elements probably arising from the dried

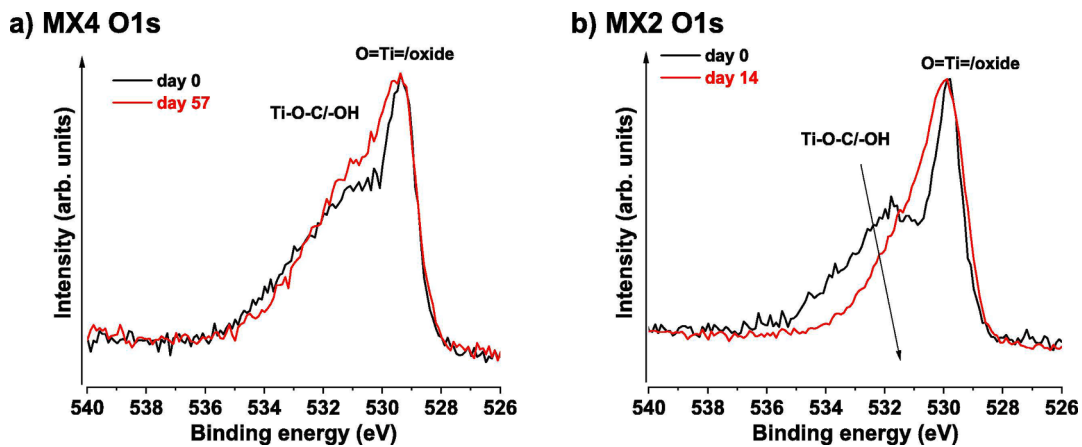


Fig. 4. XPS for the O 1s region after several days of aging for a) MX4 paste film and b) MX2 paste in air.

Table 4

Stoichiometry of MXene samples after aging for a varying number of days in air, as determined by XPS.

Days	Stoichiometry				
	MX1	2DMX1	MX2	MX3	MX4
0	Ti ₃ C _{1.91} F _{1.15} O _{1.48}	Ti ₃ C _{1.91} F _{1.19} O _{1.46}	Ti ₃ C _{1.97} F _{1.44} O _{0.68}	Ti ₃ C _{2.01} F _x O _{1.39}	Ti ₃ C _{1.82} F _x O _{1.14}
7				Ti ₃ C _{1.85} F _x O _{1.39}	
15/14*			Ti ₃ C _{1.79} F _{0.90} O _{1.54}		Ti ₃ C _{2.07} F _x O _{1.19}
21					Ti ₃ C _{2.07} F _x O _{1.39}
27/29*				Ti ₃ C _{1.77} F _x O _{2.23}	Ti ₃ C _{2.02} F _x O _{1.40}
43					Ti ₃ C _{2.16} F _x O _{1.48}
57					Ti ₃ C _{2.14} F _x O _{1.34}
83		Ti ₃ C _{1.94} F _{1.15} O _{1.42}			
337			MX2*		
			Ti ₃ C _{2.03} F _{1.66} O _{0.73}		

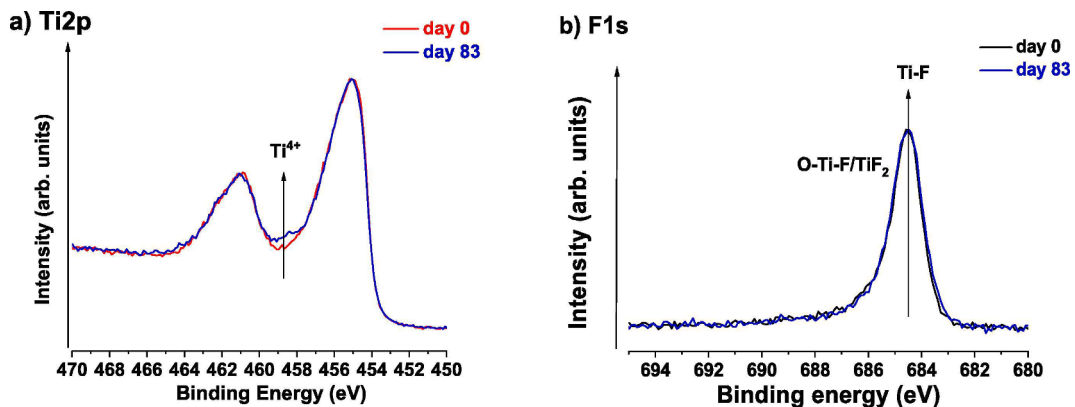


Fig. 5. XPS for 2DMX1 aging of the a) Ti 2p region and b) F1s region.

solution (Cl and Fe), and a small amount of Si at 1.74 keV, which can be attributed to the fluorescence from the Si detector [30]. Standardless TEM/EDX spectroscopy yields only semiquantitative results [31], but it is possible to monitor a ratio of selected elements as a function of time to estimate possible chemical changes in samples. In our case, an increasing O:Ti ratio (Fig. 7b) confirms gradual oxidation of the sample in air. This corresponds with the XPS results (Table 4), although the numerical values for the O:Ti ratios obtained from EDX spectroscopy are different from those obtained from XPS due to the semiquantitative nature of the standardless TEM/EDX analysis.

3.2.3. TEM/SAED: Impact of aging on MXene crystalline structure

Fig. 8 displays the key results obtained from TEM/SAED analysis. The input data for the analysis are the powder electron diffraction

patterns (insets in Fig. 6d–f), which correspond to the thicker layers of MXene platelets formed on the flat supporting carbon film. The upper graph (Fig. 8a) illustrates that the crystalline structure of MXenes does not change significantly during aging in air. Each MXene sample was measured at least twice (because we investigated two independent series of samples) and at three times (immediately after preparation, after one month, and after four months). Fig. 8a shows a representative selection of all measurements after background subtraction and radial averaging. An important conclusion is that all the TEM/SAED diffraction patterns shown in Fig. 8a are dominated by two strong MXene peaks, accompanied by a few lower-intensity diffractions. The additional lower-intensity diffractions can be attributed either to weaker MXene diffractions (peaks marked as M) or to a small amount of anatase, which is the most common crystalline modification of TiO₂ (peaks marked as A).

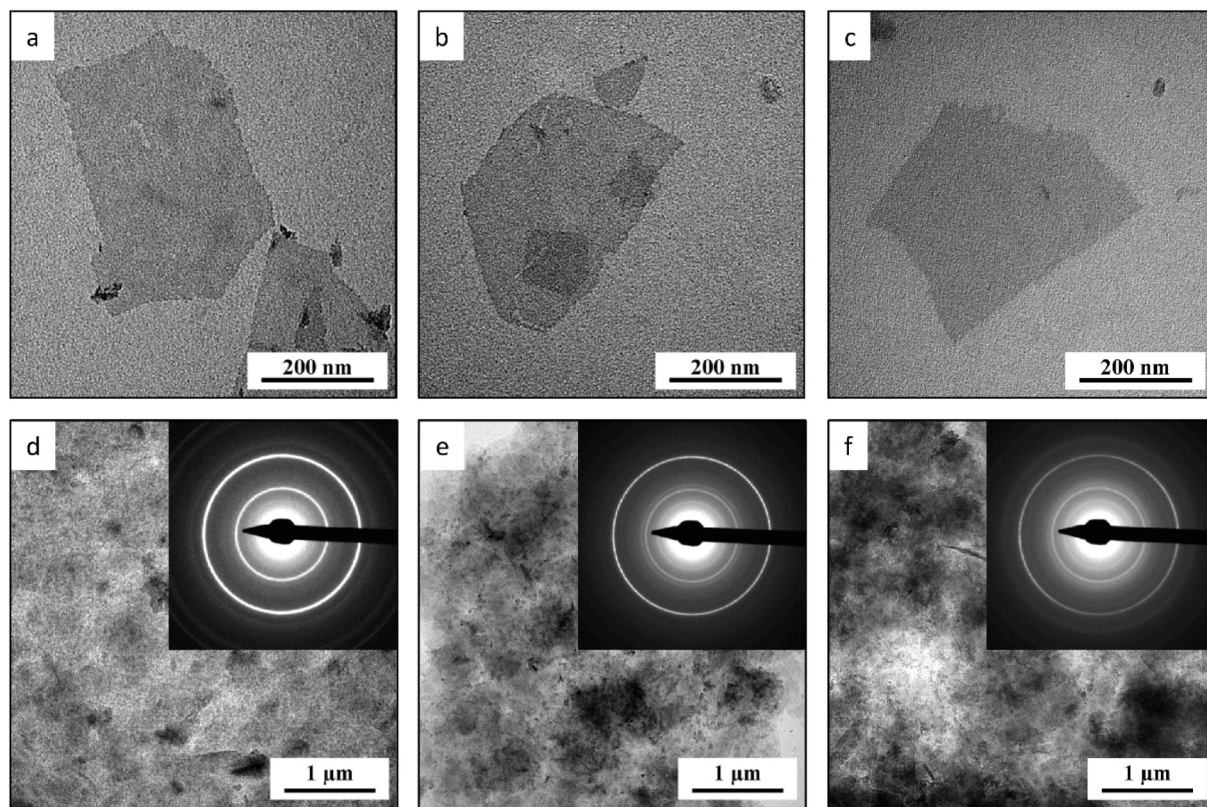


Fig. 6. TEM/BF micrographs for MX3-TEM of (a–c) single MXene platelets and (d–f) thin layers of overlapping MXene platelets. Micrographs were taken (a, d) immediately after sample preparation, (b, e) 1 month after sample preparation, and (c, f) 4 months after sample preparation. The insets in the lower row show the TEM/SAED patterns for a given sample; the patterns were normalized to approximately the same intensity for the central spot.

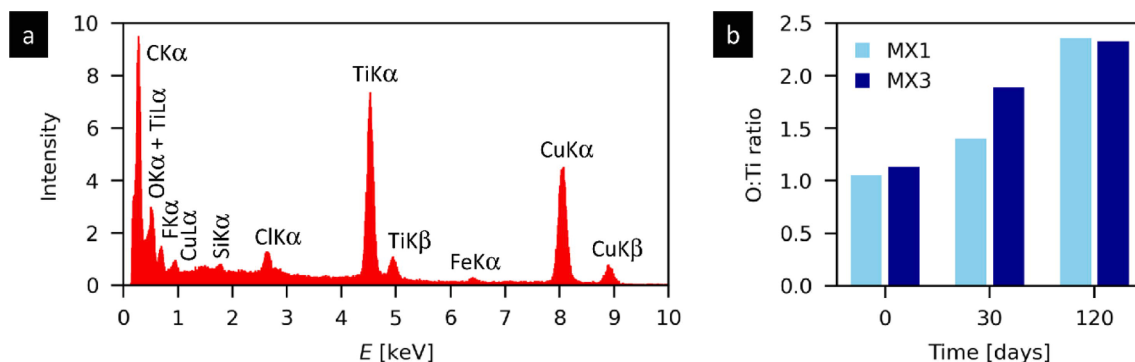


Fig. 7. TEM/EDX analysis of MXene samples: (a) representative EDX spectrum of MXene and (b) ratio of the oxygen and titanium concentration (in atomic %) for the first (light blue, MX1-TEM) and second (dark blue, MX3-TEM) series of samples.

These diffraction peaks are almost invisible in the experimental TEM-SAED pattern (as documented in the insets of Fig. 6d–f), but they can be extracted after careful background subtraction. All electron diffraction patterns were normalized to the most intense MXene diffraction peak at $q \sim 4.2 \text{ \AA}^{-1}$, and the results suggest that the intensity of additional anatase peaks tends to increase with aging time, although the results are somewhat scattered, depending on the specific location on the sample. Nevertheless, this trend corresponds to the experimentally observed fading intensity of the main MXene peaks and the appearance of additional anatase peaks in the two-dimensional TEM/SAED patterns (insets in Fig. 6d–f).

The origin of the diffraction peaks is explained in Fig. 8b, which compares the experimental TEM/SAED pattern with the theoretically calculated PXRD patterns for MXene and anatase. The PXRD patterns for both MXene and anatase exhibit many intensive diffraction peaks, but

the experimentally observed TEM/SAED patterns show only two very strong peaks and a few lower-intensity diffraction peaks. The reason why the diffraction patterns are dominated by just two peaks is the low concentration of anatase (which is why all anatase diffraction peaks show a quite low intensity) and an extremely strong preferred orientation for MXene platelets on the supporting carbon film (which is why only a few specific MXene diffraction peaks can be observed in the TEM/SAED results). Due to their two-dimensional nature, almost all MXenes lie parallel to the carbon film and perpendicular to the electron beam. Considering that the flat layers of Ti_6C octahedra forming the MXene layered structure are oriented perpendicular to the c -axis [24], the c -axis of the MXene crystals is oriented parallel to the electron beam and acts as a zone axis [32]. The MXene c -axis represents a crystallographic direction $[uvw] = [001]$. The electron diffraction pattern for the crystals oriented with the zone axis $[uvw]$ must obey the Weiss Zone Law (WZL;

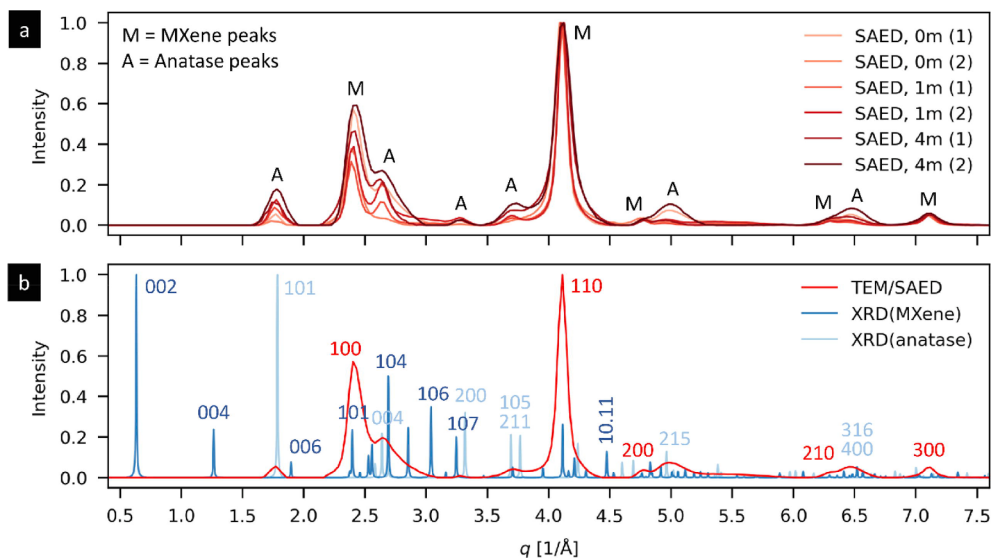


Fig. 8. TEM/SAED analysis of MXene samples: (a) Radially averaged experimental electron diffraction patterns for samples obtained from two independent syntheses taken immediately after sample preparation, one month after sample preparation, and four months after sample preparation. (b) Comparison of the representative experimental SAED pattern (red) with the calculated PXRD patterns obtained for MXene (dark blue) and anatase (light blue).

ref. [32]). The general formula for the WZL is $hu + kv + lw = 0$, where (h, k, l) are the diffraction indices and (u, v, w) are the indices of the zone axis. For our specific case of zone axis $[uvw] = [001]$, the WZL is reduced to the simple form ($l = 0$), and as a result, only the $(hk0)$ diffraction peaks (i.e., diffraction peaks with $l = 0$) are expected to appear in the SAED results. This is in perfect agreement with the experimental observation: all the MXene diffraction peaks shown in Fig. 8b (red hkl indices) are of the $hk0$ type, while no diffraction for the general type (hkl) with $l \neq 0$ is observed; even if they appear strong in the theoretical PXRD pattern (blue hkl indices). This discrepancy follows from the fact that the theoretically calculated PXRD patterns are based on randomly oriented crystals, while the experimental SAED patterns result from the real MXene sample with the extremely strong preferred orientation. The remaining weak diffraction peaks shown in Fig. 8b can be attributed to anatase (light blue hkl indices). More details concerning zone axes, WZL and SAED interpretation can be found elsewhere [32,33]. In this contribution, we conclude that the agreement between the experimental TEM/SAED and calculated PXRD patterns confirm that all observed samples are MXene nanoplatelets with a small amount of TiO_2 . The relative concentration of TiO_2 tends to increase with aging time, which can be attributed to a slow oxidative degradation of MXene to some amorphous phases (a decrease in the relative MXene concentration) or due to a slow oxygen-induced conversion of MXene to anatase (an increase in the relative anatase concentration).

Most of the TEM/SAED diffractograms display diffraction rings because the MXene sheets are all strongly oriented perpendicular to the e-beam direction (z -direction) but randomly oriented in the plane of the supporting carbon film (xy -direction). Fig. 9 shows a spotty, monocrystalline-like electron diffraction pattern arising from a special location that contains a layer composed of a few MXene sheets aligned not only in the z -direction but also in the xy -direction. Indexation of this pattern confirms the strong preferred orientation with the zone axis $[001]$ because all observed MXene diffraction peaks are of the $(hk0)$ type (the MXene diffraction peaks are compared in Fig. 8b and 9). The diffraction pattern shown in Fig. 9 is analogous to the diffractograms reported elsewhere for single MXene sheets [34].

4. Conclusion

XPS study of $\text{Ti}_3\text{C}_2\text{O}_{x}\text{F}_x$ MXene shows that it is not just the presence of oxygen that accelerates the degradation of the MXene structure but

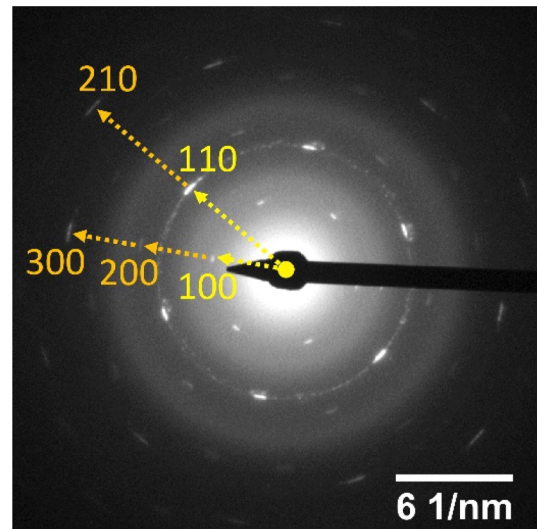


Fig. 9. Indexation of monocrystalline-like diffraction patterns for MXene platelets. Only the indices for symmetrically independent reflections are marked. The diffuse rings arise from the amorphous carbon supporting layer, onto which the MXene platelets are deposited.

also the presence of water plays an important role in the hydrolysis and degradation reactions. Progressive development of the Ti^{4+} state accompanied by the development of TiO_2 formation leads to slow disintegration of the 2D MXene nanosheets, although their overall morphology and crystalline structure can persist for several months.

TEM in multiple modes (bright field imaging, EDX, SAED) confirms the oxidation and development of TiO_2 in the anatase conformation. The presence of a LiF delamination agent does not lead to any noticeable differences in the overall stability of MXenes in air. Our XPS and TEM study documents how the surface chemistry can change during aging in air and that the Ti-F and Ti=O surface termination groups are indicators for non-oxidized $\text{Ti}_3\text{C}_2\text{O}_{x}\text{F}_x$ MXene. Moreover, we demonstrate that the storage of MXene at lower temperatures up to -20°C can result in the stabilization of MXene platelets for more than a year.

Declaration of Competing Interest

The authors declare that they have no known competing financial interests or personal relationships that could have appeared to influence the work reported in this paper.

Data availability

Data will be made available on request.

Acknowledgments

This work was supported by the Slovak Research and Development Agency under the projects APVV 19-0465, APVV-SK-BY-RD-19-0011 and Belarusian Republican Foundation for Fundamental Research under grant № X20CJIKT-004 and from agency VEGA 02/00006/22 (Slovakia). This work has received funding from the European Union's Horizon 2020 program, grant agreement No 777810. We greatly appreciate Prof. Yury Gogotsi and Dr. Christopher Shuck of Drexel University for providing the MXene paste and Oleksiy Gogotsi of MRC, Ukraine for providing the MAX phase. MS would like to thank J. Hromadkova for TEM data collection.

References

- [1] M. Ghidiu, M.R. Lukatskaya, M.Q. Zhao, Y. Gogotsi, M.W. Barsoum, Conductive two-dimensional titanium carbide 'clay' with high volumetric capacitance, *Nature* 516 (2014) 78–81, <https://doi.org/10.1038/nature13970>.
- [2] C. Zhang, M.P. Kremer, A. Seral-Ascaso, S.H. Park, N. McEvoy, B. Anasori, Y. Gogotsi, V. Nicolosi, Stamping of flexible, coplanar micro-supercapacitors using MXene inks, *Adv. Funct. Mater.* 28 (2018) 1705506, <https://doi.org/10.1002/adfm.201705506>.
- [3] Y. Xie, M. Naguib, V.N. Mochalin, M.W. Barsoum, Y. Gogotsi, X. Yu, K.W. Nam, X. Q. Yang, A.I. Kolesnikov, P.R. Kent, Role of surface structure on Li-ion energy storage capacity of twodimensional transition-metal carbides, *J. Am. Chem. Soc.* 136 (2014) 6385–6394, <https://doi.org/10.1021/ja501520b>.
- [4] H. Tang, W. Li, L. Pan, C.P. Cullen, Y. Liu, A. Pakdel, D. Long, J. Yang, N. McEvoy, G.S. Duesberg, et al. In situ formed protective barrier enabled by sulfur@ titanium carbide (MXene) inks for achieving high-capacity, long lifetime Li-S batteries. *Adv. Sci.* 5 (2018), 1800502. *Adv. Sci.* 5 (2018), 1800502. <https://doi.org/10.1002/advs.201800502>.
- [5] S. Chertopalov, V.N. Mochalin, Environment sensitive photoresponse of spontaneously partially oxidized Ti3C2Tx MXene thin films, *ACS Nano* 12 (2018) 6109–6116, <https://doi.org/10.1021/acsnano.8b02379>.
- [6] K. Chaudhuri, M. Alhabeb, Z. Wang, V.M. Shalaev, Y. Gogotsi, A. Boltasseva, Highly broadband absorber using plasmonic titanium carbide (MXene), *ACS Photonics* 5 (2018) 1115–1122, <https://doi.org/10.1021/acspophotonics.7b01439>.
- [7] U.K. Aryal, M. Ahmadpour, V. Turkovic, H.G. Rubahn, A. Di Carlo, M. Madsen, 2D materials for organic and perovskite photovoltaics, *Nano Energy* 94 (2022) 106833, <https://doi.org/10.1016/j.nanoen.2021.106833>.
- [8] F. Shahzad, M. Alhabeb, C.B. Hatter, B. Anasori, S. ManHong, C.M. Koo, Y. Gogotsi, Electromagnetic interference shielding with 2D transition metal carbides (MXenes), *Science* 353 (2016) 1137–1140, <https://doi.org/10.1126/science.aag2421>.
- [9] B. Anasori, M.R. Lukatskaya, Y. Gogotsi, 2D metal carbides and nitrides (MXenes) for energy storage, *Nat. Rev. Mater.* 2 (2017) 16098, <https://doi.org/10.1038/natrevmats.2016.98>.
- [10] A.D. Dillon, M.J. Ghidiu, A.L. Krick, J. Griggs, S.J. May, Y. Gogotsi, M.W. Barsoum, A.T. Fafarman, Highly Conductive Optical Quality Solution-Processed Films of 2D Titanium Carbide, *Adv. Funct. Mater.* 26 (2016) 4162–4168, <https://doi.org/10.1002/adfm.201600357>.
- [11] S. Huang, V.N. Mochalin, Hydrolysis of 2D transition-metal carbides (MXenes) in colloidal solutions, *Inorg. Chem.* 58 (2019) 1958–1966, <https://doi.org/10.1021/acs.inorgchem.8b02890>.
- [12] M. Naguib, M. Kurtoglu, V. Presser, J. Lu, J. Niu, M. Heon, L. Hultman, Y. Gogotsi, M.W. Barsoum, Two-dimensional nanocrystals produced by exfoliation of Ti3AlC2, *Adv. Mater.* 23 (2011) 4248–4253, <https://doi.org/10.1002/adma.201102306>.
- [13] M. Alhabeb, K. Maleski, B. Anasori, P. Lelyukh, L. Clark, S. Sin, Y. Gogotsi, Guidelines for synthesis and processing of two-dimensional titanium carbide (Ti3C2Tx MXene), *Chem. Mater.* 29 (2017) 7633–7644, <https://doi.org/10.1021/acs.chemmater.7b02847>.
- [14] M. Ghidiu, M.R. Lukatskaya, M.Q. Zhao, Y. Gogotsi, M.W. Barsoum, Conductive two-dimensional titanium carbide "clay" with high volumetric capacitance, *Nature* 516 (2014) 78–U171, <https://doi.org/10.1038/nature13970>.
- [15] A. Lipatov, M. Alhabeb, M.R. Lukatskaya, A. Boson, Y. Gogotsi, A. Sinitskii, Effect of Synthesis on Quality, Electronic Properties and Environmental Stability of Individual Monolayer Ti3C2 MXene Flakes, *Adv. Electron. Mater.* 2 (2016) 1600255, <https://doi.org/10.1002/aelm.201600255>.
- [16] O. Mashtalir, M. Naguib, V.N. Mochalin, Y. Dall'Agnese, M. Heon, M.W. Barsoum, Y. Gogotsi, Intercalation and delamination of layered carbides and carbonitrides, *Nat. Commun.* 4 (1) (2013), <https://doi.org/10.1038/ncomms2664>.
- [17] O. Mashtalir, M.R. Lukatskaya, M.Q. Zhao, M.W. Barsoum, Y. Gogotsi, Amine-assisted delamination of Nb2C MXene for Li-Ion energy storage devices, *Adv. Mater.* 27 (2015) 3501–3506, <https://doi.org/10.1002/adma.201500604>.
- [18] M. Naguib, R.R. Unocic, B.L. Armstrong, J. Nanda, Large-scale delamination of multi-layers transition metal carbides and carbonitrides "MXenes", *Dalton Trans.* 44 (2015) 9353–9358, <https://doi.org/10.1039/C5DT01247C>.
- [19] A. Iqbal, J. Hong, Y.T. Ko, C.M. Koo, Improving oxidation stability of 2D MXenes: synthesis, storage media, and conditions, *Nano Convergence* 8 (2021) 9, <https://doi.org/10.1186/s40580-021-00259-6>.
- [20] X. Sang, Y. Xie, M.-W. Lin, M. Alhabeb, K.L. Van Aken, Y. Gogotsi, P.R. Kent, K. Xiao, R.R. Unocic, Atomic Defects in Monolayer Titanium Carbide (Ti3C2Tx) MXene, *ACS Nano* 10 (2016) 9193–9200, <https://doi.org/10.1021/acsnano.6b05240>.
- [21] C.J. Zhang, S. Pinilla, N. McEvoy, C.P. Cullen, B. Anasori, E. Long, S.-H. Park, A. Seral-Ascaso, A. Shmeliov, D. Krishnan, C. Morant, X. Liu, G.S. Duesberg, Y. Gogotsi, V. Nicolosi, Oxidation stability of colloidal two-dimensional titanium carbides (MXenes), *Chem. Mater.* 29 (11) (2017) 4848–4856.
- [22] J.L. Labar, Electron Diffraction Based Analysis of Phase Fractions and Texture in Nanocrystalline Thin Films, Part I: Principles, *Microsc. Microanal.* 14 (2008) 287–295, <https://doi.org/10.1017/S1431927608080380>.
- [23] W. Kraus, G. Nolze, POWDER CELL - a program for the representation and manipulation of crystal structures and calculation of the resulting X-ray powder patterns, *J. Appl. Crystallogr.* 29 (1996) 301–303, <https://doi.org/10.1107/S002898995014920>.
- [24] C. Shi, M. Beidaghi, M. Naguib, O. Mashtalir, Y. Gogotsi, S.J.L. Billinge, Structure of Nanocrystalline Ti3C2 MXene Using Atomic Pair Distribution Function, *Phys Rev Lett* 112 (2014), 125501, <https://doi.org/10.1103/PhysRevLett.112.125501>.
- [25] V. Gajdosová, L. Lorencová, M. Procházka, M. Mičušk, M. Omastová, S. Procházková, F. Květoň, M. Jerigová, D. Velič, P. Kasák, J. Tkáč, Remarkable differences in the voltammetric response towards hydrogen peroxide, oxygen and Ru(NH3)6 3+ of electrode interfaces modified with HF or LiF-HCl etched Ti3C2Tx MXene, *Microchim. Acta* 187 (2020) 52, <https://doi.org/10.1007/s00604-019-4049-6>.
- [26] Avantage, version 5.9929; XPS knowledge database; Thermo Fisher Scientific Inc., East Grinstead, UK.
- [27] J. Halima, K.M. Cook, M. Naguib, P. Eklund, Y. Gogotsi, J. Rosen, M.W. Barsoum, X-ray photoelectron spectroscopy of select multi-layered transitionmetal carbides (MXenes), *Appl. Surf. Sci.* 362 (2016) 406–417, <https://doi.org/10.1016/j.apsusc.2015.11.089>.
- [28] M.R. Lukatskaya, J. Halim, B. Dyatkin, M. Naguib, Y.S. Buranova, M.W. Barsoum, Y. Gogotsi, Room-temperature carbide-derived carbon synthesis by electrochemical etching of MAX phases, *Angew. Chem. Int. Ed. Engl.* 53 (2014) 4877–4880, <https://doi.org/10.1002/anie.201402513>.
- [29] C.H. Peng, X. Yang, Y. Li, H. Yu, H. Wang, F. Peng, Hybrids of Two-Dimensional Ti3C2 and TiO2 Exposing 001 Facets toward Enhanced Photocatalytic Activity, *ACS Appl. Mater. Interfaces* 8 (2016) 6051–6060, <https://doi.org/10.1021/acsmami.5b11973>.
- [30] D.B. Williams, C.B. Carter, Transmission Electron Microscopy, 2nd ed. Springer, New York 2009.
- [31] D. Brandon, W.D. Kaplan (Eds.), *Microstructural Characterization of Materials*, Wiley, 2008.
- [32] K.W. Andrews, D.J. Dyson, S.R. Keown, Interpretation of Electron Diffraction Patterns. Plenum Press, New York, 1967.
- [33] U. Kostiv, O. Janouskova, M. Slouf, N. Kotov, H. Engstova, K. Smolkova, P. Jezek, D. Horak, Silica-modified monodisperse hexagonal lanthanide nanocrystals: synthesis and biological properties, *Nanoscale* 7 (2015), 18096–18104. doi: [10.1039/c5nr05572e](https://doi.org/10.1039/c5nr05572e).
- [34] R. Li, L. Zhang, L. Shi, P. Wang, MXene Ti3C2: An Effective 2D Light-to-Heat Conversion Material, *ACS Nano* 11 (2017) 3752–3759, <https://doi.org/10.1021/acsnano.6b08415>.